Image deconvolution using a characterization of sharp images in wavelet domain

Hui Ji[a,*], Jia Li[a], Zuowei Shen[a], Kang Wang[a]

[a]*Department of Mathematics, National University of Singapore, Singapore, 117542*

Abstract

Image deconvolution is a challenging ill-posed problem when only partial information of the blur kernel is available. Certain regularization on sharp images has to be imposed to constrain the estimation of true images during the blind deconvolution process. Based on the observation that an image of sharp edges tends to minimize the ratio between the ℓ_1 norm and the ℓ_2 norm of its wavelet frame coefficients, we propose a new characterization of sharp images for image deconvolution. A two-stage method is then developed to solve semi-blind image deconvolution problems. The proposed method is fast, easy to implement and does not require rigorous parameter tune-up. Such a regularization can also be applied to solve non-blind image deconvolution problems and the resulting algorithm achieves good performance without rigorous parameter tune-up.

Key words: image deconvolution, wavelet tight frame

1. Introduction

Image blurring is one of the prime causes of poor quality in digital images. A blurred image is usually modeled as the convolution of a clear image with a blur kernel plus image noise:

$$\mathbf{f} = \mathbf{h} * \mathbf{u} + \mathbf{n}, \tag{1.1}$$

where "*" denotes the discrete convolution operator, $\mathbf{f}$ denotes the available blurry image, $\mathbf{u}$ denotes the true sharp image, $\mathbf{h}$ denotes the blur kernel and $\mathbf{n}$ denotes image noise. Image deconvolution is about how to estimate the true sharp image $\mathbf{u}$ from the given blurry image $\mathbf{f}$. Depending on the availability of the blur kernel $\mathbf{h}$, existing image deconvolution methods can be classified into two categories: *non-blind* image deconvolution and *blind* image deconvolution. Non-blind image deconvolution assumes that both the blurry image $\mathbf{f}$ and the kernel $\mathbf{h}$ are available and only the true image $\mathbf{u}$ need to be estimated. Blind

*Corresponding author. Tel.: +65-65168845, Fax: +65-67795452

Email addresses: matjh@nus.edu.sg (Hui Ji), lijia@nus.edu.sg (Jia Li), matzuows@nus.edu.sg (Zuowei Shen), wangkang@nus.edu.sg (Kang Wang)

image deconvolution needs to simultaneously recover both true image $\mathbf{u}$ and blur kernel $\mathbf{h}$ from the given blurry image $\mathbf{f}$.

1.1. Non-blind image deconvolution

Non-blind image deconvolution problem is a well-known ill-conditioned inverse problem in image restoration. The high-frequency components of images are attenuated in the blurring process such that it is hard to discriminate them from the noise. To overcome such noise sensitivities when reversing convolution process, certain image prior has to be imposed to constrain the estimation of true image. Let f, u, h denote the column-wise vector forms of $\mathbf{f}, \mathbf{u}, \mathbf{h}$ respectively and let $\otimes$ denote the convolution operator under the vector form. Then, in the presence of Gaussian white image noise, a pre-defined image prior usually is enforced by formulating the image deconvolution as the following minimization problem:

$$\min_{u\in\mathbb{R}^n} \Psi(u), \quad s.t. \quad \|h\otimes u - f\|_2 \leq \eta, \tag{1.2}$$

where Ψ is the regularization term that imposes the image prior on the image u and η is the error tolerance dependent on the noise level. Or, in a Langrangian regularization form, the minimization becomes

$$\min_{u\in\mathbb{R}^n} \frac{1}{2}\|h\otimes u - f\|_2^2 + \lambda\Psi(u),$$

where λ is the regularization parameter.

An ideal regularization term for image deconvolution should have its minimizer exactly equal to an image with sharp edges. Thus, we need to give an accurate quantitative definition on what is a nature image with sharp edges. Earlier works on non-blind image deconvolution impose various smooth priors on images which assume natural images can be approximated by a smooth function. This type of smooth image priors leads to the so-called Tikhonov regularizations ([1]) which regularize the image by minimizing its ℓ_2 norm of image gradients: $\Psi(u) = \|\Gamma u\|_2^2$, where Γ is some first-order or higher-order difference operator. The edges of the results from the Tikhonov regularization tend to be smoothed out such that the result still looks blurry. Then the piece-wise smooth image prior was introduced to regularize images without smoothing image edges, which resulted in the so-called total variation (TV) regularization: $\Psi(u) = \|\Gamma u\|_1$, where Γ is also some first-order or higher-order difference operator. Such a TV regularization and its variations have been used not only in image deconvolution but also in many other image restoration tasks (e.g. [2, 3, 4, 5]).

Recently, sparsity-based image prior has emerged in many image restoration tasks as one promising approach. The sparsity-based image prior assumes that natural images are very likely to be sparse under certain transform domain, i.e., most coefficients of the image under the transform are zero or close to zero. One representative transform is *wavelet tight frame* transform, including shift-invariant wavelet transform [6], framelet [7, 8] and many others. The sparsity-based image prior usually is enforced via minimizing the ℓ_1 norm of

transform coefficients of the true image: $\Psi(u) = \|Wu\|_1$, where W denotes the wavelet tight frame transform. Framelet is chosen in [9, 10] to sparsify images in the applications of image deblurring. Impressive results are reported in their experiments. In fact, the popular TV measure is essentially a special and simplest case of $\|Wu\|_1$ if we take appropriate method of discretization, as proved in [11].

1.2. Blind image deconvolution

In practice, it is more often that the blur kernel is either completely unknown or only its partial information is available. In such a case, both the true image and the blur kernel need to be estimated and we call it a blind image deconvolution problem. Blind deconvolution problem is a much more challenging ill-posed inverse problem, as the bi-linear system (1.1) is under-constrained and there exist an infinite number of mathematically sound solutions. Similar to non-blind deconvolution, to overcome the ill-posedness of blind deconvolution problem, we also need to impose certain image prior on true images. Moreover, since the information on blur kernel is not complete, some additional prior on the blur kernel is needed to constrain the blur kernel.

The prior on the blur kernel varies with different types of image blurring. Based on how blur kernels are mathematically expressed, there are two types of blind image deconvolution: semi-blind deconvolution and complete blind deconvolution. Semi-blind deconvolution assumes that blur kernels can be expressed by some parametric function. For example, Bar et al. [12] used isotropic Gaussian functions of unknown width to approximate the kernel of optical blurring. Ji et al. [13] used line segments with unknown orientation and length to approximate the kernel of motion blurring caused by simple camera shakes. Complete blind image deconvolution usually uses an regularization term to constrain blur kernels, the same as images. For example, TV regularization [2] for constraining optical blurring; and the sparsity prior of kernels under curvelet domain [14] for constraining complex motion-blur kernels.

The regularizations on images used in most existing blind image deconvolution methods are essentially the same as those used in non-blind deconvolution methods. For example, the TV regularization is used in [2] to regularize images in their blind deconvolution method; and the sparsity-based prior of images under framelet transform is used in [14] to regularize images. In recent years, some other image regularizations are proposed to regularize images when remove motion blurring from images, e.g., the heavy-tailed prior of image gradients which assumes the image gradients obey heavy-tailed distributions [15] and a normalized TV regularization for images [16].

1.3. Motivation and our main contributions

In this paper, we are interested in how to regularize images for blind and non-blind image deconvolutions, primarily focusing on blind deconvolution. One main challenge in blind image deconvolution is about how to overcome the ambiguities between true image u and kernel h. Taking, for example, an image

blurred by a Gaussian blur kernel $h_\sigma = \frac{1}{2\pi\sigma^2}\exp(-\frac{x^2+y^2}{2\sigma^2})$. We have $f = h_\sigma \otimes u$. Notice that $h_{\sigma_1} \otimes h_{\sigma_2} = h_{(\sigma_1^2+\sigma_2^2)^{1/2}}$. For $t<0$, Let h_t denote the inverse filter of h_{-t} defined by $h_t \otimes h_{-t} = \delta$. Then, all the following pairs (u^*, h^*) are also the solutions of the bi-linear system (1.1):

$$\{u^*, h^*\} = \{h_t \otimes u, h_{(\sigma^2-t^2)^{1/2}}\}, \quad 0 \le t \le \sigma,$$

where t denotes the kernel error. Thus, the solution u^* from (1.1) can be either under-deblurred with $u^* = h_t \otimes u, t>0$; or over-deblurred with $u^* = h_t \otimes u, t<0$.

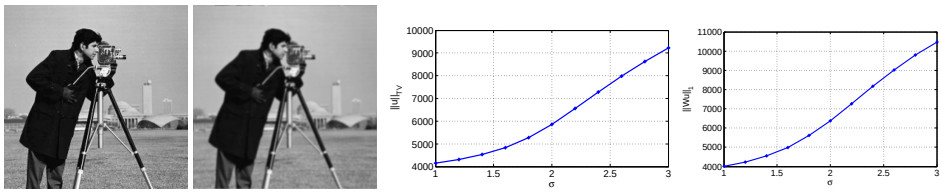

(a) (b) (c) (d)

Figure 1: The illustration of $\|\Gamma u\|_1$ and TV for both over- and under-deblurred results. (a) true image; (b) blurry image blurred by Gaussian kernel with $\sigma = 2$; (c) graph of $\|\Gamma u\|_1$ of deblurred results using kernel with different variances; (d): graph of $\|Wu\|_1$ of deblurred results using kernel with different variances. Images are deblurred using Wiener Filter.

An ideal regularization for blind deconvolution should reject all those results $h_t \otimes u$ with non-zero t. However, many existing regularizations, e.g. TV measure $\|\Gamma u\|_1$ and sparsity measure $\|Wu\|_1$, can only reject those over-deblurred results $h_t \otimes u$ with $t<0$ but not under-deblurred results $h_t \otimes u$ with $t>0$. In other words, the true image with sharp edges is not corresponding to the minimum point of the cost function $\Psi(u)$. See Fig. 1 for a visual illustration. To avoid the convergence to an under-deblurred solution, one then has to implement some additional regularization on blur kernels to maximize the width of blur kernel (e.g. [12]). However, such an ad-hoc approach requires, for each input, rigorous tune-up on the regularization parameter associated with such an additional regularization to obtain the correct result. There is no an universal optimal parameter setting as the optimal values of the regularization parameters are closely related to the blurring degree which varies with different images.

This paper aims at developing a new characterization of sharp images for blind deconvolution such that the minimizer of the resulting cost function $\Psi(u)$ is exactly an image with sharp edges. Such a new cost function will greatly help the development of new blind deconvolution methods that do not need additional ad-hoc constraints on blur kernels and do not need troublesome parameter tune-up. The new characterization is based on the empirical observation that an image with sharp edges tends to minimize the ratio between the ℓ_1 norm and the ℓ_2 norm of its wavelet coefficients. To demonstrate the power of the proposed new cost function, we developed a fast two-stage method for solving semi-blind image deconvolution problems with respect to various types of blur kernels. The experiments showed the proposed two-stage method performed

much better than existing methods on tested data sets. Moreover, a preliminary study is carried on to also use such an characterization to solve non-blind image deconvolution problems and the resulting method achieved a modest gain on the performance compared against other state-of-art methods and it is much less sensitive to the setting of regularization parameters.

2. New characterization of sharp images under wavelet tight frame

2.1. Brief review on wavelet tight frame and ℓ_1 norm-based regularization

Motivated by the impressive performance of wavelet tight frame based methods in image deconvolution (e.g. [17, 14, 10]), we also use the wavelet tight frame coefficients of images to build a new characterization of images with sharp edges. Before presenting our proposed image regularization for image deconvolution, we briefly review a few facts of discrete tight wavelet frame decomposition and reconstruction. Interesting readers should consult [8] for theories of frames and framelets and [18, 19] for a more detailed survey. In the discrete setting, an image is a 2D array that can be understood as a vector living in $\mathbb{R}^n$, with n the total number of pixels in the image. Then the discrete wavelet tight frame decomposition and reconstruction can be represented as matrix multiplications W and $W^\top$ respectively, where W is derived by the wavelet filters obtained by the unitary extension principle. Here $W \in \mathbb{R}^{k\times n}$ satisfies $W^\top W = I$, i.e. $u = W^\top W u$, $\forall u \in \mathbb{R}^n$. The decomposition operator W usually is composed of one low-pass filtering operator W_0 and multiple high-pass filtering operators $\{W_j\}_{j=1}^L$ in a multi-scale fashion: $W = [W_0^\top, W_1^\top \ldots, W_L^\top]^\top$. It is noted that The matrix multiplications by W and $W^\top$ are only for the notational convenience. In the implementation, these two matrix multiplications are done by using the fast tensor product tight wavelet frame decomposition and reconstruction algorithms instead, which are essentially just the convolution of images by a set of filters (see e.g. [19]).

The proposed cost function is closely related to that used in those wavelet tight frame based deconvolutions ([17, 14, 10]). These methods assume that an image with sharp edges is very likely to have a sparse cardinal expansion under wavelet tight frame systems. In other words, the vector of wavelet tight frame coefficients of a sharp image u, denoted by Wu, is sparse such that most elements of Wf are zero or close to zero. Such an assumption can be approximately measured by the ℓ_1 norm of wavelet coefficients $\|Wu\|_1$, which leads to the following minimization for image deconvolution:

$$\min_{u\in\mathbb{R}^n} \|Wu\|_1 \quad s.t. \quad \|h\otimes u - f\|_2 \le \eta. \tag{2.1}$$

2.2. New characterization of sharp images for blind image deconvolution

The ℓ_1 norm based measure $\|Wu\|_1$ works well for non-blind deconvolution. However, for blind deconvolution, $\|Wu\|_1$ is not an ideal candidate for constraining a sharp image as the sharp image is not a well-defined minimum point of $\|Wu\|_1$. The phenomena illustrated in Fig. 1 is not surprising. The same as

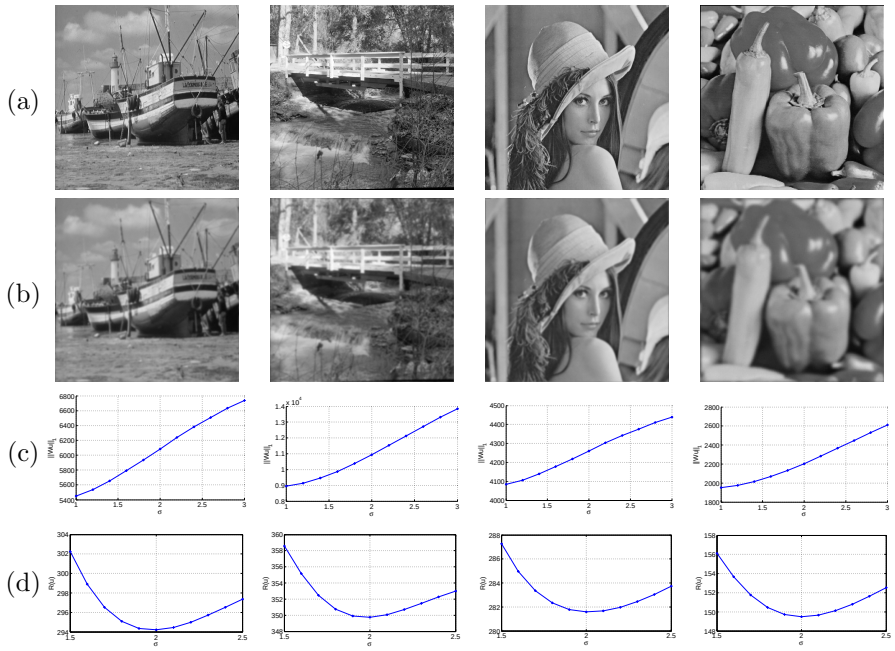

Figure 2: (a): true images; (b): images blurred by Gaussian kernel with $\sigma = 2.0$; (c): graphs of $\|Wu\|_1$ of results deblurred by kernels with different variances. (d): graphs of $\mathcal{R}$ of results deblurred by kernels with different variances. Images are deblurred using Wiener filter.

the ℓ_2 norm, the ℓ_1 norm of an image will also decrease when being blurred by a low-pass filter because high frequency components of the image are attenuated by the low-pass filter.

The above observation leads us to propose the following image measure to constrain a sharp image:

$$\mathcal{R}(u) := \frac{\sum_{i\neq 0} \|W_i u\|_1}{\sum_{i\neq 0} \|W_i u\|_2}, \tag{2.2}$$

where $W_i u$ denotes the wavelet tight frame coefficient vector of u in i-th high-pass channel. For a given clear image u, It is empirically observed (See Fig. 2) that the measure $\mathcal{R}$ is a better cost function to constrain sharp images, as $\mathcal{R}(h_t \otimes u)$ is a unimodal function with the minimum point of t close to 0 (corresponding to sharp image). Owing to its unimodality w.r.t. kernel error t, the measure $\mathcal{R}$ provides us a powerful constraint on sharp images. Based on the new cost function $\mathcal{R}$, we can build up simple yet effective blind image deconvolution methods. It is noted that a similar TV-based concept is also used in [16] to remove non-uniform motion blurring from photographs.

3. Two-stage semi-blind deconvolution method

Based on the proposed cost function $\mathcal{R}$, we developed a fast two-stage method to solve the so-called semi-blind image deconvolution problem (e.g. [12, 13]). As we stated earlier, certain prior information of blur kernels is necessary to overcome the ill-posedness of blind deconvolution. Many typical image blurrings have been well studied and their parametric forms are established. For example, Gaussian functions for representing the kernels of out-of-focus blurring, and line segments for representing the kernels of linear motion blurring cause by simple camera shakes. Such an image deconvolution problem is the so-called *semi-blind* deconvolution problem which assumes that the blur kernel can be approximated by some functional form with unknown physical parameters. In other words, we have the following equation with unknowns p and u:

$$f = H(p)u + n, \tag{3.1}$$

where $H(p)$ denotes the convolution matrix determine by the kernel with the parameter vector p. The goal of the semi-blind deconvolution is to simultaneously estimate both p and u.

Other existing methods usually solve (3.1) through an iterative scheme which alternatively refines the estimations of the kernel and the true image. That is, during each iteration, using the current estimation of the image to estimate the blur kernel and using the updated estimation of the blur kernel to re-estimate the image. Such an alternating scheme is known to be very slow and the convergence is not guaranteed. Owing to the nice properties of the measure function $\mathcal{R}$, we proposed a fast two-stage semi-blind approach:

1. First, the kernel parameter vector p is directly estimated by using the measure function $\mathcal{R}$;
2. Based on the estimated blur kernel, the true image is recovered by using some non-blind deconvolution method such as the one proposed in [20].

The second step in the proposed two-stage approach is rather straightforward. We focus on the first step, i.e., how to directly estimate the direct the blur kernel. It is seen in Fig. 2 that the sharp image u is very close to the minimum point of the unimodal function $\mathcal{R}(h_t \otimes u)$ w.r.t. t. Thus, a simple strategy to identify the true blur kernel is to find the kernel parameters whose corresponding deblurred image minimizes $\mathcal{R}$, which leads to the following minimization model:

$$\min_{p\in\mathbb{R}^\ell} \mathcal{R}\big[(H(p)^\top H(p) + \tau W_h^\top W_h)^{-1}(H(p)^\top f)\big], \tag{3.2}$$

where $W_h = (W_1; W_2; \ldots, W_L)$ denotes the matrix representing all wavelet high-pass filtering operations. It is seen from (3.2) that the term inside $\mathcal{R}[\cdot]$ actually is the deblurred image u with respect to the kernel with parameter p, and the image is deblurred by using the following Tikhonov regularization:

$$u(p) = \operatorname{argmin}_{u\in\mathbb{R}^n} \frac{1}{2}\|H(p)u - f\|_2^2 + \frac{1}{2}\tau\|W_h u\|_2^2, \tag{3.3}$$

where $\tau\|W_h u\|_2^2$ is mainly for stabilizing the non-blind deconvolution process. The value of τ has little impact on the accuracy of the kernel estimation.

It is noted that the deblurring method (3.3) used in this stage is using the ℓ_2 norm based regularization, which is different from the deblurring method used in the next stage. Recall that our goal is to identify correct blur kernel. Thus, the deblurring method used to generate the corresponding result should have the following two properties: 1) it should be very fast as it may be called for many times; 2) it should not be robust to errors in blur kernel as it may break the unimodality of $\mathcal{R}(h_t \otimes u)$. The above two requirements lead to the usage of ℓ_2 norm based instead of ℓ_1 norm based regularization. Actually, many other non-iterative deblurring method will work as well.

In a quick glance, the minimization (3.2) seems complicated. However, the unimodality of $\mathcal{R}(h_t \otimes u)$ in a wide neighborhood of the minimum point, shown in Fig. 2, actually makes (3.2) rather easy to solve. We propose to use the *golden section search* method [21] owing to its global convergence. The golden section search method is to find the minimum point of the given function by successively narrowing the range of values inside which the minimum point is known to exist. The classic golden section search method is designed only for one-dimensional case. We extended the golden section search method to the multi-dimensional case. The basic idea is to use a recursive scheme, i.e., change one variable at a time to improve the estimation of the bounding cube while the other variables are held constant, then the problem is reduced to a sequence of sub-optimization problems of lower-dimension which can be recursively solved by applying the same golden search method. The detailed multi-dimensional search algorithm is outlined in Alg. 1.

Algorithm 1 Recursive multi-dimensional Golden Section Search for solving $\min_{x\in\Omega\subset\mathbb{R}^n} f(x)$

Step 0. Set the initial bounding cube of the solution $\Omega = \prod_{i=1}^{n}[a^{(i)}, b^{(i)}]$ and set the desired precision ϵ. Denote this procedure by $gssn(f, \Omega, n, \epsilon)$.

Step 1. Perform $gssn(f, \Omega, n-1, \epsilon)$ on each dimension $(i = 1, ..., l)$ alternatively by the following procedure until $\max_i(b_i - a_i) \le \epsilon$:

$$
\begin{cases}
\text{For} \quad i = 1, ..., n \\
\quad x_1 := gssn(f, \Omega_1, n-1, \epsilon) \text{ where } \Omega_1 = \{x \in \Omega, x^{(i)} = a^{(i)} + 0.382 * (b^{(i)} - a^{(i)})\} \\
\quad x_2 := gssn(f, \Omega_2, n-1, \epsilon) \text{ where } \Omega_2 = \{x \in \Omega, x^{(i)} = x_1^{(i)} + 0.382 * (b^{(i)} - x_1^{(i)})\} \\
\quad a^{(i)} := \begin{cases} x_1^{(i)} & \text{if } f(x_1) > f(x_2); \\ a^{(i)} & \text{otherwise.} \end{cases} ; \quad b^{(i)} := \begin{cases} b^{(i)} & \text{if } \quad f(x_1) > f(x_2); \\ x_2^{(i)} & \text{otherwise.} \end{cases}
\end{cases}
$$

Step 3. The optimal parameter is taken as $\hat{x} := \frac{a+b}{2}$.

---

4. $\mathcal{R}$-inspired non-blind image de-convolution

After the blur kernel is given, the remained task is to robustly deblur images in the presence of image noise. The existing wavelet frame based non-blind deconvolution methods (e.g. [20]) use the ℓ_1 norm of wavelet coefficients of the image as the regularization term:

$$\min_{u\in\mathbb{R}^n} \frac{1}{2}\|Hu-f\|_2^2+\lambda\|W_h u\|_1, \tag{4.1}$$

where H denotes the convolution matrix and λ is the regularization parameter. The minimization (4.1) can be efficiently solved by the split Bregman iteration:

$$\begin{cases} u^{k+1} := (H^\top H+\mu W_h^\top W_h)^{-1}\left(H^\top f+\mu W_h^\top (d^k-b^k)\right), \\ d^{k+1} := \mathcal{T}_{\lambda/\mu}(W_h u^{k+1}+b^k), \\ b^{k+1} := b^k+(W_h u^{k+1}-d^{k+1}). \end{cases} \tag{4.2}$$

Impressive results have been reported in [20]. However, like many other regularization methods, the value of the regularization parameter λ in (4.1) is very important to the performance of the split Bregman iteration. Unfortunately, in practice, the optimal value of λ varies with different types of images. The goal of this section is then to develop a new regularization method that is much less sensitive to the value of the regularization parameter.

The introduction of the new cost function $\mathcal{R}$ not only greatly facilitates the development of blind deconvolution methods, as we showed in the the previous section, but also it can benefit the regularization based non-blind deconvolution methods, particularly regarding the choice of regularization parameters. However, directly using $\mathcal{R}$ may lead to a challenging minimization problem. Notice that $\mathcal{R}$ is essentially about avoiding the case in which ℓ_1 norm of wavelet coefficients is minimized by decreasing the value of its ℓ_2 norm. Thus, we proposed the following approximate minimization model:

$$\min_u \frac{1}{2}\|Hu-f\|_2^2+\lambda\sum_{i\neq 0}\|W_i u\|_1 \quad \text{s.t.} \quad \|W_i u\|_2 \geq c_i, \quad i=1,2,\ldots,L. \tag{4.3}$$

where c_i is the energy of the image in each high-pass wavelet channel. Clearly, the value of c_i is dependent on the true image u. We proposed a heuristic approach to iteratively update the value of c_i when solving (4.3) by split Bregman iteration. The detailed algorithm for solving (4.3) with the built-in updating mechanism of c_i is described in Algorithm 2.

5. Experiments and discussion

5.1. Evaluation of Algorithm 1

In this section, the performance of Algorithm 1 is evaluated for various types of image blurring. Four representative types of image blur kernel are tested in

Algorithm 2 Algorithm for solving the model (4.3)

Step 0. Initialize the estimate of u using the split Bregman iteration for several iterations. Set the u^0, d^0, b^0 as the outputs from the split Bregman iteration.
Step 1. Set up an auxiliary variable $q^0 = 0$ and set $c_i^0 = \|W_i u^0\|_2$ for $1 \le i \le L$.
Step 2. For $k = 1, 2, \ldots$, perform the following iteration until $\|Hu - f\|_2 \le \epsilon$

$$\begin{cases} c_i^{k+1} := (1+10^{-3})\max(c_i^k, \|W_i u^k\|_1), \quad i = 1, 2, \ldots, L. \\ u^{k+1} := (H^\top H + \mu W_h^\top W_h + \mu_2 \sum_{i \neq 0} q_i W_i^\top W_i)^{-1} \\ \qquad \left(H^\top (f - h^k) + \mu W_h^\top (d^k - b^k)\right), \\ d^{k+1} := \mathcal{T}_{\lambda/\mu}(W_h u^{k+1} + b^k), \\ b^{k+1} := b^k + (W_h u^{k+1} - d^{k+1}), \\ q^{k+1} := \max(0, q^k - (\|W_h u^{k+1}\|_2 - c^{k+1})), \end{cases} \tag{4.4}$$

where μ and μ_2 are two parameters ($\mu = 10^{-2}$ and $\mu_2 = 10^{-6}$ in our setting).

the experiments, including Gaussian kernel, disk kernel, box kernel and linear motion kernel. The isotropic Gaussian blur kernel, with variance parameter σ^2, has explicit mathematical expression as $h_\sigma = \frac{1}{2\pi\sigma^2} \exp(-\frac{x^2+y^2}{2\sigma^2})$. The other three blur kernels can be expressed as

$$h = \begin{cases} 1 & \textit{for pixels in } \Omega, \\ 0 & \textit{otherwise}, \end{cases}$$

where Ω is disk region, box region and line segment for disk blurring, box blurring and linear motion blurring, respectively. See Fig. 3 for the illustration of these four kernels with their corresponding physical parameters. The tested images are generated by first applying the blur kernel on them and then adding additional Gaussian white noise with various standard deviation (std).

The visualization of $\mathcal{R}(h_t \otimes u)$ of sampled images with respect to different blur kernels are shown in Fig. 4. The unimodality of $\mathcal{R}(h_t \otimes u)$ is clearly demonstrated on these sample images. It is seen that the minimum points of these functions are very close to the true blur kernels. Algorithm 1 are extensively evaluated on these images with different kernels and different parameter values. It is seen from Table 1 that the parameters estimated by our algorithm are nearly exact. Clearly, these experiments showed the validity of $\mathcal{R}$ for characterizing nature images with sharp edges.

5.2. Comparison against other semi-blind de-convolution methods

The existing semi-blind deconvolutions mostly focus on how to deblur images blurred by Gaussian blur kernels. In the experiments, our proposed method is compared against two other methods: one is the TV-based blind deconvolution method proposed by [2]; and another is the one proposed by Bar et al. [12]. The method proposed in [2] used TV measure to regularize both images and blur kernels. Similar to Bar et al. [12], we also modified the blind deconvolution

Blur Type	Gaussian	Disk	Box	Motion
Kernel				
Parameter	variance σ	disk radius	length & width	length & orientation

Figure 3: The illustration of four types of blur kernels tested in the experiments.

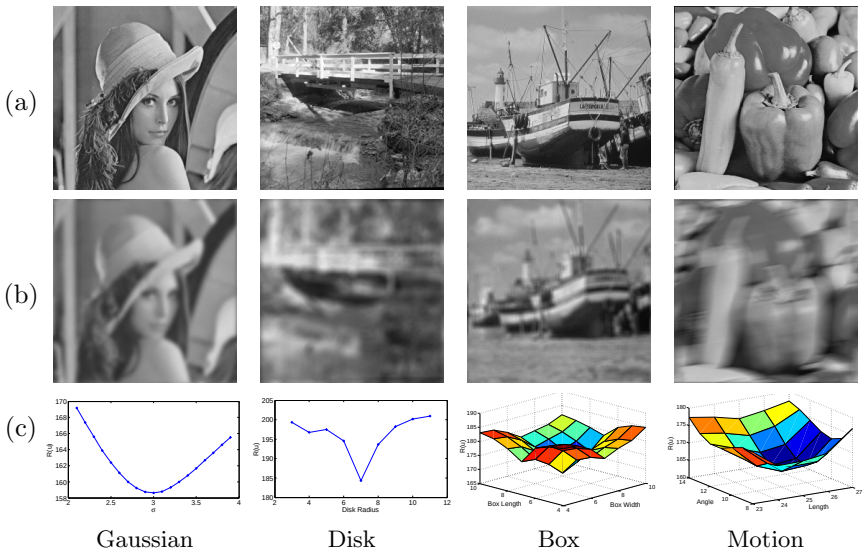

Figure 4: Visualization of $\mathcal{R}$ w.r.t. different blur kernels. (a): truth images; (b): images blurred by four types of blur kernels with Gaussian white noise with $std = 1$; (c): graphs of $\mathcal{R}$ of deblurred results for the corresponding images in (b) using kernels with different parameters.

model proposed in [2] by restricting the kernel in the class of isotropic Gaussian Blur kernels:

$$\min_{u,\sigma} \frac{1}{2}\|H(\sigma)u - f\|_2^2 + \lambda\|\nabla u\|_1 + \mu F(\sigma) \tag{5.1}$$

where σ is the variance parameter the isotropic Gaussian blurring kernel, $H(\sigma)$ is the convolution matrix of the Gaussian kernel with variance σ. F is a decreasing function of σ that prompts blur kernel with larger variance, such that the minimizer is away from an under-deblurred solution ($F(\sigma) = -\sigma$ in our implementation). There are two parameters in (5.1): one is regularization parameter λ that regularizes the image and the other is the regularization parameter μ for the kernel. The model of (5.1) is not convex and an alternating iterative scheme is used to solve u and σ. That is, during each iteration, the estimate of u is updated using the split Bregman iteration where σ is obtained from the previous step; and the estimate of σ is updated by directly searching the minimizer of (5.1) where u is the most recent estimate.

Table 1: Kernel parameter estimation in the presence of Gaussian white noise with $\sigma = 2$

kernel	Gaussian		disk		box		motion	
true value	2	3	7	10	[7,7]	[9,11]	$[15, 30^\circ]$	$[25, 10^\circ]$
lena	2.10	3.01	7	10	[7,7]	[9,11]	$[15, 28^\circ]$	$[25, 10^\circ]$
boat	2.01	3.00	7	10	[7,7]	[9,11]	$[15, 31^\circ]$	$[25, 10^\circ]$
bridge	2.01	2.97	7	10	[7,7]	[9,11]	$[15, 30^\circ]$	$[25, 11^\circ]$
peppers	2.04	3.01	7	10	[7,7]	[9,11]	$[15, 30^\circ]$	$[25, 10^\circ]$

In the experiments, the results from (5.1) are compared against that from our proposed method. The two parameters in (5.1) are rigorously tuned up for all images to achieve optimal performance. The tested images are generated by first applying the Gaussian blur kernel with different variances, followed by adding the additional Gaussian white noise. See Table 1 for the results of kernel parameter estimation. It is clear that the proposed method yielded much more accurate estimations of kernels and the resulted images are also of better quality in terms of PSNR value. The visual comparison between ours and (5.1) on sampled images is shown in Fig. 5. It is seen that the results from (5.1) tend to slightly under-deblurred as the image edges are less shape than that from our methods. More importantly, our method does not require any parameter tune-up while the model (5.1) requires rigorous parameter tune-up to achieve its optimal performance.

Figure 5: Comparison of deblurred results of sample images blurred by Gaussian blurring kernel ($\sigma = 2$) in the presence of Gaussian white noise with std=1. Images shown in the first row and the second row are results using the model from [2] and using our model respectively.

The method proposed by Bar et al. [12] also attempted to better constrain sharp images to avoid the under-deblurred solution, which is done by incorporating the Mumford-Shah segmentation model. Similarly, the alternating iterative scheme is used to solve the resulting minimization model. It is noted that due to the implementation complexity of [12], the results used in the comparison

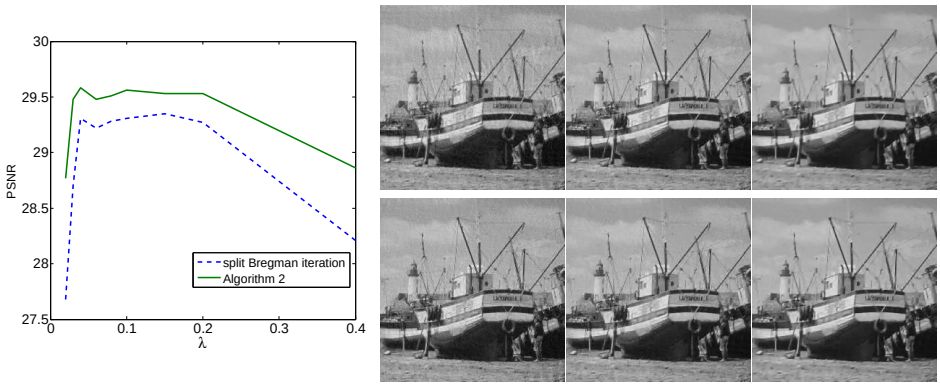

Comparison of PSNR values (a) | $\lambda = 0.02$ (b) | $\lambda = 0.1$ (c) | $\lambda = 0.4$ (d)

Figure 6: Results for the image "boat" blurred by a linear blur kernel with the parameter $[15, 30°]$. (a): The graph of the PSNR values of deblurred results for image "boat" using different settings of λ. (b) – (d): results using different regularization value λ. The first row and the second row are results by split Bregman iteration and by Algorithm 2 respectively.

.

are directely from [12]. Clearly, it is seen from Table 2 that our method outperformed [12] in terms of PSNR value. Also, our implementation is much simpler than that of [12] and ours does not require any parameter tune-up.

Table 2: Comparison of kernel parameter estimation between [12] and Alg. 1

	coin	coin1	lena	cameraman	einstein	sail
true value	2.10	2.10	2.10	2.10	2.10	2.60
Bar et al. [12]	2.05	1.77	2.01	1.95	2.27	2.57
Alg. 1	2.09	2.10	2.10	2.09	2.08	2.61

5.3. Evaluation of Algorithm 2

Similar to the split Bregman iteration, there is still one parameter λ in Algorithm 2 for solving (4.3). However, the setting of λ in Algorithm 2 is much less sensitive than that of the split Bregman iteration. It is seen from Fig. 6 (a) that Algorithm 2 can keep a steady high PSNR value (> 29.2) when λ is in the range from 0.03 to 0.3 while the split Bregman iteration achieves similar performance in a much narrow range. See Fig. 6 (b) – (d) for a visual comparison of results from both algorithms.

6. Conclusion

In this paper, based on wavelet tight frame coefficients of images, we proposed a new characterization of sharp images that provides a more accurate

constrain on images with sharp edges. Based on this new chracterization, we proposed a two-stage semi-blind image deconvolution method that is very simple to implement and requires no parameter tune-up. It is shown in the experiments that the proposed two-stage method outperformed existing TV-based semi-blind deconvolution techniques in tested images. Moreover, it also can be used in the non-blind deconvolution method with small modifications. The resulting non-blind deconvolution method yielded modest gains in image quality and does not require rigorous parameter tune-up for optimal performance as many existing regularization based image deconvolution methods do.

References

[1] A. Tikhonov, V. Arsenin, F. John, Solutions of ill-posed problems, VH Winston Washington, DC, 1977.

[2] T. Chan, C. Wong, Total variation blind deconvolution, IEEE Transactions on Image Processing 7 (3) (1998) 370–375.

[3] T. Chan, A. Marquina, P. Mulet, High-order total variation-based image restoration, SIAM J. Sci. Comput. 22 (2000) 503–516.

[4] T. Chan, J. Shen, Image Processing and Analysis: Variational, PDE, Wavelet, and Stochastic Methods, SIAM, 2005.

[5] Q. Shan, J. Jia, A. Agarwala, High-quality motion deblurring from a single image, ACM Transactions on Graphics 27 (3) (2008) 73–73.

[6] R. Coifman, D. Donoho, Translation-invariant de-noising, in: Lecture Notes in statistics, Springer Verlag, 1995, pp. 125–125.

[7] A. Ron, Z. Shen, Affine Systems in $L_2(\mathbb{R}^d)$: The Analysis of the Analysis Operator, Journal of Functional Analysis 148 (2) (1997) 408–447.

[8] I. Daubechies, B. Han, A. Ron, Z. Shen, Framelets: Mra-based constructions of wavelet frames, Applied and Computational Harmonic Analysis 14 (1) (2003) 1–46.

[9] J. Cai, Z. Shen, Framelet based deconvolution, J. Comp. Math 28 (3) (2010) 289–308.

[10] J. Cai, S. Osher, Z. Shen, Linearized Bregman iterations for frame-based image deblurring, SIAM J. Imaging Sci. 2 (1) (2009) 226–252.

[11] J. Cai, B. Dong, S. Osher, Z. Shen, Image restorations: total variation, wavelet frames and beyond, preprint.

[12] L. Bar, N. Sochen, N. Kiryati, Semi-blind image restoration via mumford-shah regularization, IEEE Trans. Image Processing 15 (2) (2006) 483–493.

[13] H. Ji, C. Liu, Motion blur identification from image gradients, in: CVPR, 2008.

[14] J. Cai, H. Ji, C. Liu, Z. Shen, Blind motion deblurring from a single image using sparse approximation, in: CVPR, 2009.

[15] R. Fergus, B. Singh, A. Hertzmann, S. Roweis, W. Freeman, Removing camera shake from a single photograph, in: ACM SIGGRAPH, 2006.

[16] D. Krishnan, T. Tay, R. Fergus, Blind deconvolution using a normalized sparsity measure, in: CVPR, 2011.

[17] J. Cai, R. Chan, Z. Shen, A framelet-based image inpainting algorithm, Applied and Computational Harmonic Analysis 24 (2) (2008) 131–149.

[18] Z. Shen, Wavelet frames and image restorations, in: International Congress of Mathematicians, India, 2010.

[19] B. Dong, Z. Shen, Mra based wavelet frames and applications, IAS Lecture Notes Series, Summer Program on "The Mathematics of Image Processing", Park City Mathematics Institute.

[20] J. Cai, S. Osher, Z. Shen, Split Bregman methods and frame based image restoration, Multiscale Modeling and Simulation: A SIAM Interdisciplinary Journal 8 (2) (2009) 337–369.

[21] J. Kiefer, Sequential minimax search for a maximum, Proceedings of the American Mathematical Society 4 (3) (1953) 502–506.